Improved Stability and Photoluminescence Yield of Mn²⁺-Doped $CH_3NH_3PbCl_3$ Perovskite Nanocrystals

Xianli Li [1,2,†], **Yan Guo** [1,2,†] **and Binbin Luo** [1,2,*] (iD)

[1] Department of Chemistry, Shantou University, Guangdong 515063, China; lixianli@stu.edu.cn (X.L.); 17yguo1@stu.edu.cn (Y.G.)
[2] Department of Chemistry and Key Laboratory for Preparation and Application of Ordered Structural Materials of Guangdong Province, Shantou University, Guangdong 515063, China
* Correspondence: bbluo@stu.edu.cn
† These authors contributed equally to this work.

Abstract: Organic–inorganic $CH_3NH_3PbCl_3$ perovskite nanocrystals (PNCs) doped with Mn²⁺, $CH_3NH_3Pb_xMn_{1-x}Cl_3$, have been successfully prepared using a reprecipitation method at room temperature. Structural and morphological characterizations reveal that the $CH_3NH_3Pb_xMn_{1-x}Cl_3$ PNCs with cubic phase transforms from particles to cubes and increases in size from 16.2 ± 4.4 nm in average diameter to 25.3 ± 7.2 nm in cubic length after the addition of Mn²⁺ precursor. The $CH_3NH_3Pb_xMn_{1-x}Cl_3$ PNCs exhibit a weak exciton emission at ~405 nm with a low absolute quantum yield (QY) of around 0.4%, but a strong Mn²⁺ dopant emission at ~610 nm with a high QY of around 15.2%, resulting from efficient energy transfer from the PNC host to the Mn²⁺ dopant via the $^4T_1 \rightarrow {}^6A_1$ transition. In addition, the thermal and air stability of $CH_3NH_3Pb_xMn_{1-x}Cl_3$ PNCs are improved due to the passivation with (3-aminopropyl) triethoxysilane (APTES), which is important for applications such as light emitting diodes (LEDs).

Keywords: perovskite; Mn²⁺ doping; $CH_3H_3PbCl_3$; stability

1. Introduction

As a promising candidate for photovoltaics and lighting application, lead halide perovskite (LHP) afford many intriguing advantages over traditional semiconductor materials such as simple fabrication [1–4], abundant precursors source, defect tolerance [5,6], high photoluminescence (PL) quantum yields (QY) [5,7–9], halogen dependent emission over the entire visible spectral range with narrow full width at half maximum (FWHM) [10,11], as well as long carrier lifetime and diffusion length [12]. Compared with the intensive investigations of lead bromide and iodide perovskite [13–17], lead chloride perovskites have received less attention due to its low PL QY and large bandgap (~2.97 eV), which is less desirable for light emitting diodes (LEDs) and solar cells applications [18].

Doping metal ions into nanocrystals is an effective approach to tuning their optical, electronic and magnetic properties, as has been widely applied to II-VI metal chalcogenide nanocrystals [19,20]. Recently, several heterovalent or isovalent metal ions such as Bi³⁺ [21], Al³⁺ [22], Sn²⁺ [23], Cd²⁺ [23], Zn²⁺ [23], and Mn²⁺ [24–30] have been introduced into LHP as dopants to modulate their optical properties. Among these metal ions, Mn²⁺-doped all inorganic $CsPbCl_3$ perovskite nanocrystals (PNCs) have attracted increasing attention owing to the appropriate band alignment of $CsPbCl_3$ and d-d transition of Mn²⁺ (2.15 eV, $^6A_1 \rightarrow {}^4T_1$), resulting in efficient intraparticle energy transfer between the host exciton and dopant ions [25,31]. Moreover, the incorporation of Mn²⁺ may provide the possibility of imparting paramagnetism to the host materials [31].

In general, hot injection approach has been applied in the preparation of Mn²⁺-doped lead halide PNCs because of the homogeneous products and relatively simple purification process [32,33].

However, the highly strict conditions of this method and poor stability of the resulting PNCs greatly hinder their applications. In contrast, organic-inorganic hybrid $CH_3NH_3PbCl_3$ PNCs can be easily prepared via solution-based reprecipitation approach at room temperature when (3-aminopropyl) triethoxysilane (APTES) is used as a capping ligand [34,35]. Additionally, the SiO_2 shell resulting from the hydrolysis of APTES capping ligand can greatly improve the product yield and stability of $CH_3NH_3PbCl_3$ PNCs towards water and air [34].

In this work, we demonstrate that Mn^{2+} can be doped into $CH_3NH_3PbCl_3$ PNCs via a reprecipitation method. By adjusting the doping concentration of Mn^{2+}, $CH_3NH_3Pb_xMn_{1-x}Cl_3$ PNCs with a strong dopant emission located at 610 nm were obtained. Besides the greatly improved overall QY of $CH_3NH_3Pb_xMn_{1-x}Cl_3$ PNCs (from ~0.4% to ~15.6%) upon Mn^{2+} doping, the thermal and air stability have also been enhanced by the SiO_2 shell formed from hydrolysis of APTES. The combined stability and high PL QY make these PNCs potentially useful for various photonics applications including LEDs.

2. Experimental Section

2.1. Materials

All the chemicals were used as received without further purification, including $PbCl_2$ (99.99%, Aladdin Chemical Co., Ltd., Shanghai, China), CH_3NH_2 (40%, TCI Chemical Co., Ltd., Tokyo, Japan), $MnCl_2$ (99%, Aladdin Chemical Co., Ltd., Shanghai, China), APTES (99%, Aladdin Chemical Co., Ltd., Shanghai, China), HCl (37.5%, Xilong Scientific Co., Ltd., Shantou, China), toluene (AR, Xilong Scientific Co., Ltd., Shantou, China), N,N-dimethylformamide (DMF, spectroscopic grade, 99.9%, Aladdin Chemical Co., Ltd., Shanghai, China), oleic acid (85%, TCI Chemical Co., Ltd., Tokyo, Japan), octylamine (99%, Fisher Scientific Co., Ltd., Pittsburgh, PA, US), ethyl acetate (99%, Aladdin Chemical Co., Ltd., Shanghai, China).

Mn^{2+}-doped $CH_3NH_3PbCl_3$ PNCs: CH_3NH_3Cl was prepared according to a reported procedure [18]. The Mn^{2+}-doped $CH_3NH_3PbCl_3$ PNCs were synthesized following a method reported previously with some small changes [1]. 1.5 mL precursor solution of PNCs was prepared by dissolving 0.05 mmol CH_3NH_3Cl, 0.05 mmol ($PbCl_2$ + $MnCl_2$), 0.05 mmol APTES or octylamine and 40 μL oleic acid in 1.5 mL DMF solvent and ultrasonicated until the solution became transparent. Then, 10 μL, 25 μL, 50 μL and 100 μL of the precursor solution were injected slowly into 5 mL toluene to form $CH_3NH_3PbCl_3$ PNCs solution. Mn^{2+}-doped $CH_3NH_3PbCl_3$ PNCs with different doping concentration of Mn^{2+} were prepared by varying the ratio between $PbCl_2$ and $MnCl_2$. The solid samples were obtained by adding ethyl acetate in toluene to precipitate $CH_3NH_3PbCl_3$ PNCs and centrifuged at 4000 rpm subsequently, then re-dispersed in toluene. These steps were repeated three times. At last, the dry samples were collected by placing the samples at 50 °C oven overnight.

Mn^{2+}-doped $CH_3NH_3PbCl_3$ PNCs films: The films were prepared by dropping purified solution on microslides and dried at room temperature.
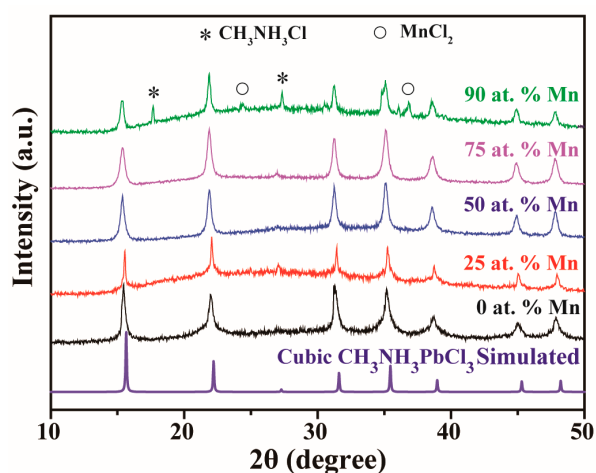
2.2. Characterization

Absorption and photoluminescence properties of the samples were collected with circular dichroism spectra (MOS450, Biologic Science Instruments, Seyssinet-Pariset, France) and fluorescence spectra (PTI QM-TM, Photon Technology International, Ontario, Canada), respectively. Absolute QY was recorded on HAMAMATSU C11347 spectrometer (Hamamatsu Photonics Instruments, Hamamatsu City, Japan) by testing samples in toluene. Luminescence lifetime measurements were collected on EDINBURGH INSTRUMENTS (FLS920, Edinburgh Instruments Ltd., Livingston, UK). X-Ray diffraction (XRD, MiniFlex 600, Rigaku Corporation, Tokyo, Japan) analysis was used to obtain the crystalline phase. The scanning angle range was 10–50° (2θ) with a rate of 3°/min. Temperature-dependent Powder XRD (Ultima IV, Rigaku Corporation, Tokyo, Japan) were studied to indicate the thermal stability of samples. Transmission electron microscopy (TEM, Tecnai G2 F20,

FEI Technologies, Hillsboro, OR, USA) were carried out to obtain the morphology and interlayer spacing of samples at an accelerating voltage of 200 kV. The elemental analysis was conducted on inductively coupled plasma atomic emission spectroscopy (ICP-AES, Agilent 720, Agilent Technologies, Santa Clara, CA, USA).

3. Results and Discussion

### 3.1. Structural and Morphological Characterizations

The structure and morphology of the prepared samples were determined by XRD and TEM measurements, respectively. For the nominal doping concentration of Mn^{2+} in 0~75 at.% range, the XRD pattern (Figure 1) shows a series of diffraction peaks that can all be attributed to cubic phase $CH_3NH_3PbCl_3$ perovskite structure (space group: $Pm\bar{3}m$), demonstrating that the incorporation of Mn^{2+} has little effect on the crystal structure of $CH_3NH_3PbCl_3$ [18]. With the addition of 90 at. % $MnCl_2$, some diffraction peaks attributed to CH_3NH_3Cl and $MnCl_2$ precursors could be clearly observed due to the excess amount of precursors. Note that the broad band ranging from 15° to 38° is characteristic of amorphous silica resulting from the hydrolysis of APTES, which has been clearly elucidated in our previous work [34]. To further determine the concentration of Mn^{2+} dopant, ICP-AES was used, with results summarized in Table S1. In the synthesis of Mn^{2+}-doped $CH_3NH_3PbCl_3$ PNCs, it was found that APTES would react with $MnCl_2$ to form a puce complex at a high concentration of Mn^{2+} precursor, as shown in Figure S1. The color of $CH_3NH_3Pb_xMn_{1-x}Cl_3$ PNCs capped with APTES under room light is deeper than that of $CH_3NH_3Pb_xMn_{1-x}Cl_3$ PNCs passivated with octylamine owing to the adsorption of Mn^{2+}-APTES complex, indicating that the detected concentration in Table S1 are higher than the actual concentration of Mn^{2+} in the crystal lattice.

Figure 1. XRD pattern of Mn^{2+}-doped $CH_3NH_3PbCl_3$ PNCs with different concentration of Mn^{2+} (nominal concentration). The asterisks and circles denote the characteristic XRD peaks of CH_3NH_3Cl and $MnCl_2$, respectively.

To determine the morphology evolution and size distribution, TEM images were recorded, as shown in Figure 2. For undoped $CH_3NH_3PbCl_3$ PNCs (Figure 2a), the PNCs are mostly spherical with an average diameter of 16.2 ± 4.4 nm. The PNCs are embedded in amorphous silica matrix (Figure S2), which results from the hydrolysis of APTES. When $MnCl_2$ precursor was added, the resulting Mn^{2+}-doped PNCs are mostly cubic with an average dimension increasing from 10.4 ± 5.1 nm (Figure 2b) to 25.3 ± 7.2 nm (Figure 2e) as the Mn^{2+} concentration was increased from 25 to 90 at. %. Due to the complex reaction between APTES and the Mn^{2+} precursor, the concentration of APTES ligands decreased after adding $MnCl_2$ precursor. Higher concentration of APTES can facilitate the formation of small spherical PNCs due to the large steric hindrance of branched APTES [34]. Likewise,

with the increase of Mn^{2+} precursor concentration, the lower concentration of APTES will result in large cubic PNCs, which is consistent with the TEM results of this work. High-resolution TEM (HRTEM, Figure 2f) reveals that the lattice space of undoped PNCs is around 0.28 nm, corresponding to the (200) crystal plane of cubic $CH_3NH_3PbCl_3$.
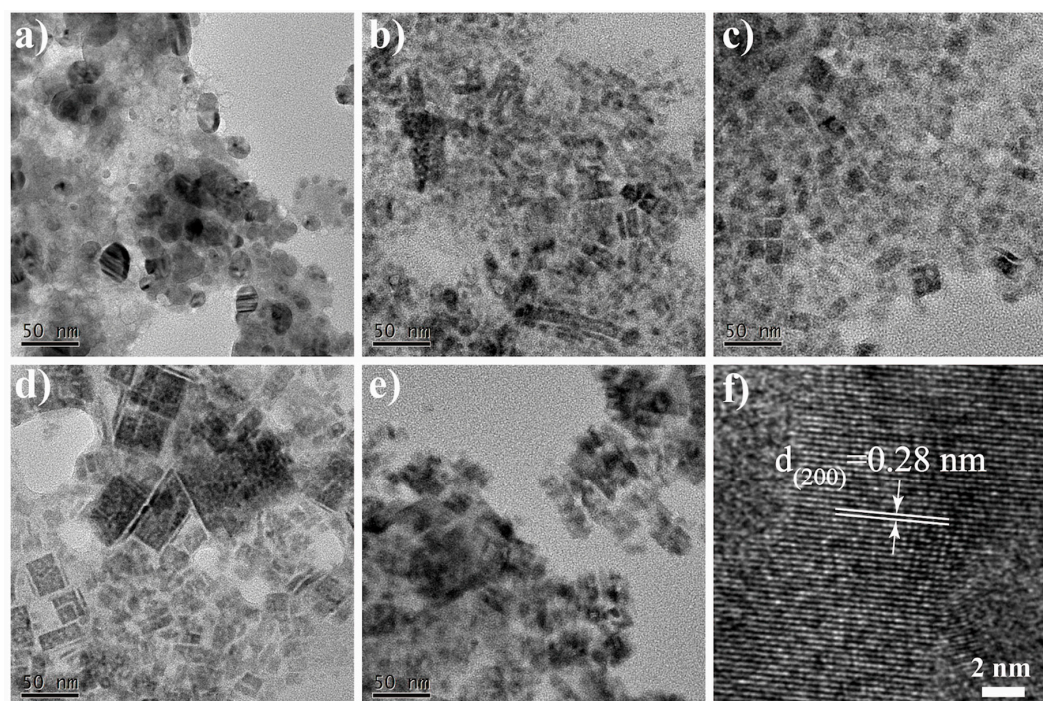
Figure 2. TEM images of Mn^{2+}-doped $CH_3NH_3PbCl_3$ PNCs doped with different Mn^{2+} concentrations. (**a**) 0 at. % Mn^{2+}, (**b**) 25 at. % Mn^{2+}, (**c**) 50 at. % Mn^{2+}, (**d**) 75 at. % Mn^{2+}, (**e**) 90 at. % Mn^{2+} and (**f**) HRTEM image of 0 at. % Mn^{2+}.

3.2. Optical Properties

Similar to Mn^{2+}-doped all inorganic $CsPbCl_3$ PNCs, new emission band may be introduced in Mn^{2+}-doped organic-inorganic $CH_3NH_3PbCl_3$ PNCs, as shown in the PL spectra in Figure 3, where the electronic absorption spectra are also shown. For undoped $CH_3NH_3PbCl_3$ PNCs, the absorption spectrum exhibits a sharp rise starting around 400 nm and an excitonic peak at ~373 nm. In comparison, the excitonic peak positions of all the Mn^{2+}-doped $CH_3NH_3PbCl_3$ PNCs shift 4–10 nm towards long wavelength owing to a significant increase in average particle size. For the PL spectra, Mn^{2+}-doped $CH_3NH_3PbCl_3$ PNCs feature a broad emission band peaked at 610 nm, attributed to the spin-forbidden $^4T_1 \rightarrow {}^6A_1$ transition of Mn^{2+} [31], along with a narrow luminescence band located at ~400 nm, which is assigned to intrinsic excitonic emission of the $CH_3NH_3PbCl_3$ host. Compared to the Mn^{2+} dopant emission (~590 nm) in $CsPbCl_3$ PNCs [28,31], Mn^{2+} dopant emission in the $CH_3NH_3PbCl_3$ system significantly red shifts by ~20 nm, possibly caused by the crystal lattice difference between cubic $CH_3NH_3PbCl_3$ and cubic/tetragonal $CsPbCl_3$. The lattice parameters of cubic $CH_3NH_3PbCl_3$ (space group: $Pm\bar{3}m$, a = b = c = 5.685 Å) are a little larger than that of cubic $CsPbCl_3$ (a = b = c = 5.605 Å) and tetragonal $CsPbCl_3$ (a = b = 5.590 Å, c = 5.630 Å) [18,36], resulting in the smaller energy difference (Δ_O) of Mn^{2+} d-orbitals.
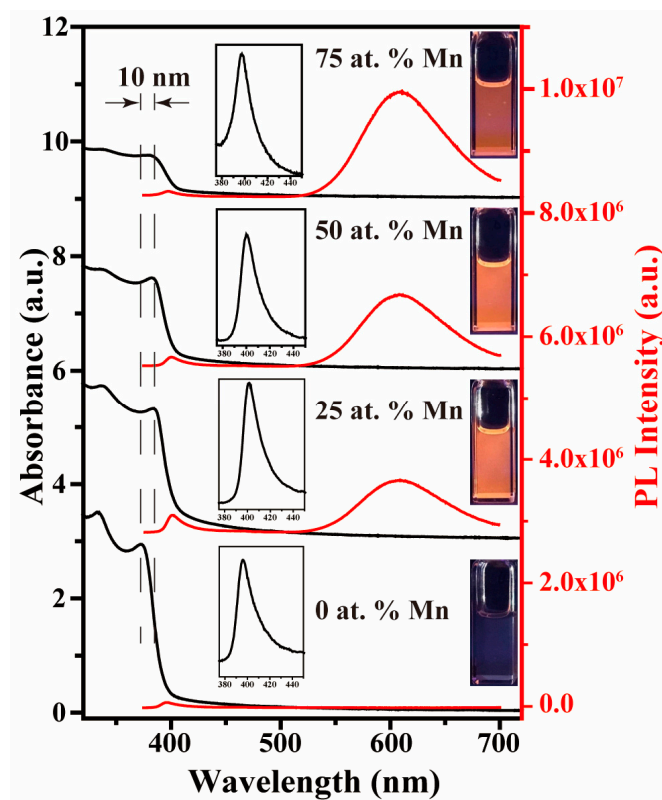
**Figure 3.** Absorption and PL spectra of Mn^{2+}-doped $CH_3NH_3PbCl_3$ PNCs solution with different nominal Mn^{2+} doping concentration. Inset: Enlarged views of PL spectra located in 375–450 nm range and digital pictures of Mn^{2+}-doped $CH_3NH_3PbCl_3$ PNCs under 365 nm UV light.

In addition, all excitonic emissions of Mn^{2+}-doped $CH_3NH_3PbCl_3$ PNCs show a slight red-shift (~4 nm) with respect to that of undoped $CH_3NH_3PbCl_3$ PNCs, consistent with red-shifted absorption spectra, attributed to the increase in size of PNCs. Intriguingly, with the increased concentration of Mn^{2+} dopant, the PL intensity of host increases first and then decreases, which is highly unusual. On one hand, the Mn^{2+} dopant ions may remove the preexisting structural defects and enhance the excitonic emission of hosts [25,37]. At the low doping concentration, both the intensity of excitionic emission and dopant emission are increased after 25 at. % Mn^{2+} doping, attributed to the dominant defect passivation of Mn^{2+} and exciton-to-Mn^{2+} energy transfer. On the other hand, the excitonic emission will be quenched upon the incorporation of Mn^{2+}. With the addition of a higher Mn^{2+} concentration, the transfer of excitonic energy from the host to Mn^{2+} dopants becomes more dominant, giving rise to the decrease of excitonic emission intensity and enhancement of dopant emission intensity. Importantly, the overall PL QY was highly improved from 0.4% (undoped) to 15.6% (75 at. % Mn^{2+}-doped), indicating efficient excitons-to-Mn^{2+} energy transfer, which is desired for light emitting applications.

To demonstrate that the Mn^{2+} dopant emission does not originate from the Mn^{2+}-APTES complex, contrast test was conducted as shown in Figure S3. Without the formation of $CH_3NH_3PbCl_3$ perovskite, no absorption and emission band can be observed. In the range of 380–700 nm, no emission can be seen for $MnCl_2$ precursor, indicating that the Mn^{2+} dopant emission results from the host absorption. In addition, PLE spectra are collected to further illustrate the emission mechanism of Mn^{2+}-doped $CH_3NH_3PbCl_3$ PNCs. As shown in Figure S4, a sharp onset located at ~400 nm can be clearly observed for all Mn^{2+}-doped $CH_3NH_3PbCl_3$ PNCs, consistent with the absorption of undoped $CH_3NH_3PbCl_3$ PNCs. These results display that the emission band centered at 610 nm originates from the absorption of $CH_3NH_3PbCl_3$ PNCs, manifesting the energy transfer from host to dopants.

The volume ratio between precursor solution and anti-solvent (toluene) is an important factor in the synthesis of $CH_3NH_3PbCl_3$ PNCs when adopting the reprecipitation strategy. Figure S5 displays the PL spectrum of Mn^{2+}-doped $CH_3NH_3PbCl_3$ PNCs solution prepared with different volume ratios. The Mn^{2+} dopant emission greatly increases in the range of 50–200 volume ratio after normalizing to excitonic emission, implying that more Mn^{2+} ions are incorporated into the crystal lattice of $CH_3NH_3PbCl_3$. However, the intensity of dopant emission is diminished when reaching 500 toluene/precursor volume ratio, owing to the poor crystallinity of the host at high Mn^{2+} dopant concentration, thereby lower the transfer efficiency of photo-induced excitons between the host and dopants due to the competition of charge transfer to trap states [28].

To investigate the PL decay of $CH_3NH_3Pb_xMn_{1-x}Cl_3$ PNCs, time-resolved PL spectra are obtained. All the PL decay kinetics were fitted with a single exponential curve, as shown in Figure 4. An expected decrease of excitonic lifetime from 2.40 ns to 2.04 ns can be observed with increasing the Mn^{2+} concentration from 0% to 75% (Figure 4a), due to the energy transfer from the host to Mn^{2+} dopants. Interestingly, the small change of exciton emission lifetime indicates the insignificant effect of dopant states on the overall exciton decay in the $CH_3NH_3PbCl_3$ PNCs. Since the introduction of Mn^{2+} dopants provides a new and efficient decay pathway of the excitons, which leads to the radiative decay of Mn^{2+} via the $^4T_1 \rightarrow {}^6A_1$ transition, the overall PL QY of the doped PNCs was improved [28].
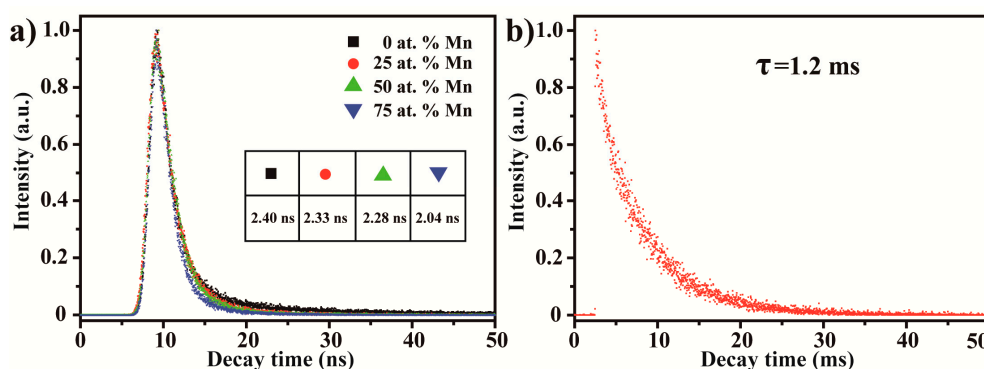
**Figure 4.** PL decay spectrum of Mn^{2+}-doped $CH_3NH_3PbCl_3$ PNCs films prepared with different $MnCl_2$ concentration. (**a**) Monitored at exciton emission (~410 nm) and (**b**) Mn^{2+} dopant emission of 50 at.% Mn (~610 nm).

PL decay curve of Mn^{2+} dopant emission located at 610 nm was also studied and presented in Figure 4b. A very long lifetime of 1.2 ms was observed resulting from the spin-forbidden nature of Mn^{2+} $^4T_1 \rightarrow {}^6A_1$ transition, suggesting the successful incorporation of Mn^{2+} [28,38].

3.3. Stability Investigation

Although moisture stability of $CH_3NH_3PbCl_3$ has been greatly improved, their practical applications are still restricted by their low decomposition temperature, which is determined by their low formation energies [39]. A recent study found that the formation energy of Mn^{2+}-doped $CsPbBr_3$ is calculated to be ~5% larger than that of pure $CsPbBr_3$ using DFT simulation, suggesting the better thermal stability of $CsPbBr_3$ after Mn^{2+} doping with a specific concentration [39]. In this work, the thermal stability of pure $CH_3NH_3PbCl_3$ and $CH_3NH_3Pb_xMn_{1-x}Cl_3$ PNCs has also been studied using temperature-dependent XRD, as presented in Figure 5. Without the addition of $MnCl_2$ precursor, $CH_3NH_3PbCl_3$ PNCs capped with octylamine (Figure 5a) show poor thermal stability. Some diffraction peaks due to impurities could be observed when the temperature was increased up to 170 °C. $CH_3NH_3Pb_xMn_{1-x}Cl_3$ PNCs passivated with octylamine were relatively stable under 170 °C, but still to be decomposed at 180 °C (Figure 5b). In contrast, both $CH_3NH_3PbCl_3$ PNCs and $CH_3NH_3Pb_xMn_{1-x}Cl_3$ PNCs passivated with APTES show better thermal stability, as shown in

Figure 5c,d. The decomposition temperature was significantly improved by 20–30 °C compared to PNCs passivated with octylamine. The improved thermal stability of $CH_3NH_3PbCl_3$ PNCs passivated with APTES may be due to the SiO_2 coating layer, which maintains the morphology and crystal structure of $CH_3NH_3PbCl_3$ as a result of the higher thermal stability of SiO_2.
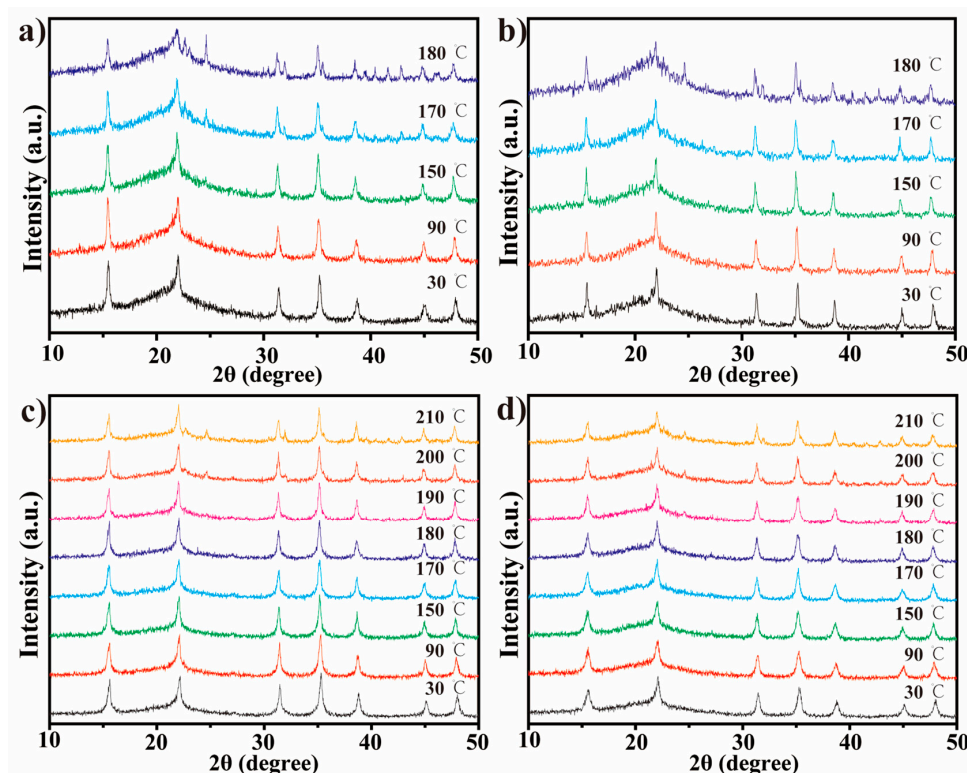
Figure 5. Temperature-dependent Powder XRD test of (**a**) $CH_3NH_3PbCl_3$ PNCs passivated with octylamine, (**b**) 50 at.% Mn^{2+}-doped $CH_3NH_3PbCl_3$ PNCs passivated with octylamine, (**c**) $CH_3NH_3PbCl_3$ PNCs passivated with APTES and (**d**) 50 at.% Mn^{2+}-doped $CH_3NH_3PbCl_3$ PNCs passivated with APTES.

The air stability of $CH_3NH_3Pb_xMn_{1-x}Cl_3$ PNCs films was also studied, as shown in Figure S6. The PL intensity $CH_3NH_3Pb_xMn_{1-x}Cl_3$ PNCs passivated with APTES and octylamine drop ~9% and ~73% after one week, indicating the better air stability of $CH_3NH_3Pb_xMn_{1-x}Cl_3$ PNCs capped with APTES.

4. Conclusions

Doping of Mn^{2+} into organic-inorganic $CH_3NH_3PbCl_3$ PNCs has been demonstrated using a versatile reprecipitation approach. The PL QY of the obtained samples are greatly improved after Mn^{2+} doping as a result of efficient energy transfer from the host to dopants. Furthermore, both thermal and air stability are enhanced due to the presence of SiO_2 on the PNC surface. Importantly, compared to the Mn^{2+} dopant emission (~590 nm) in all inorganic $CsPbCl_3$ system, the larger crystal lattice of $CH_3NH_3PbCl_3$ results in a lower energy splitting of Mn^{2+} d-orbitals, thereby emitting at a longer wavelength (~610 nm). In this manner, Mn^{2+} dopant emission may be tuned by modulating the crystal lattice through substitution of different components in perovskites.

APTES precursors (black line), and using $MnCl_2$, APTES, $PbCl_2$ and CH_3NH_3Cl precursors (red line). (c) PL spectra of $MnCl_2$ (λ_{ex} = 360 nm); Figure S4: PLE spectra of Mn doped $CH_3NH_3PbCl_3$ PNCs with different doping concentration (λ_{em} = 610 nm); Figure S5: PL spectra of 50 at.% Mn^{2+}-doped $CH_3NH_3PbCl_3$ PNCs solutions with different toluene/precursor volume ratios; Figure S6: Air stability test of Mn^{2+}-doped $CH_3NH_3PbCl_3$ PNCs passivated with octylamine and APTES; Table S1. Elemental analysis of $CH_3NH_3Pb_xMn_{1-x}Cl_3$ PNCs passivated with APTES under different doping concentration using ICP-AES.

Author Contributions: X.L. and B.L. conceived and designed the experiments; X.L. and Y.G. performed the experiments and analyzed the data; B.L. wrote the paper.

Conflicts of Interest: The authors declare no conflicts of interest.

References

1. Zhang, F.; Zhong, H.; Chen, C.; Wu, X.; Hu, X.; Huang, H.; Han, J.; Zou, B.; Dong, Y. Brightly luminescent and color-tunable colloidal $CH_3NH_3PbX_3$ (X = Br, I, Cl) quantum dots: Potential alternatives for display technology. *ACS Nano* **2015**, *9*, 4533–4542. [CrossRef] [PubMed]

2. Luo, B.; Naghadeh, S.B.; Allen, A.L.; Li, X.; Zhang, J.Z. Peptide-passivated lead halide perovskite nanocrystals based on synergistic effect between amino and carboxylic functional groups. *Adv. Funct. Mater.* **2017**, *27*, 1604018. [CrossRef]

3. Xuan, T.; Yang, X.; Lou, S.; Huang, J.; Liu, Y.; Yu, J.; Li, H.; Wong, K.; Wang, C.; Wang, J. High stable $CsPbBr_3$ quantum dots coated with alkyl phosphate for white light-emitting diodes. *Nanoscale* **2017**, *9*, 15286–15290. [CrossRef] [PubMed]

4. Konstantakou, M.; Perganti, D.; Falaras, P.; Stergiopoulos, T. Anti-solvent crystallization strategies for highly efficient perovskite solar cells. *Crystals* **2017**, *7*, 291. [CrossRef]

5. Dirin, D.N.; Protesescu, L.; Trummer, D.; Kochetygov, I.V.; Yakunin, S.; Krumeich, F.; Stadie, N.P.; Kovalenko, M.V. Harnessing defect-tolerance at the nanoscale: Highly luminescent lead halide perovskite nanocrystals in mesoporous silica matrixes. *Nano Lett.* **2016**, *16*, 5866–5874. [CrossRef] [PubMed]

6. Huang, H.; Bodnarchuk, M.I.; Kershaw, S.V.; Kovalenko, M.V.; Rogach, A.L. Lead Halide perovskite nanocrystals in the research spotlight: Stability and defect tolerance. *ACS Energy Lett.* **2017**, *2*, 2071–2083. [CrossRef] [PubMed]

7. Koscher, B.A.; Swabeck, J.K.; Bronstein, N.D.; Alivisatos, A.P. Essentially trap-free $CsPbBr_3$ colloidal nanocrystals by postsynthetic thiocyanate surface treatment. *J. Am. Chem. Soc.* **2017**, *139*, 6566–6569. [CrossRef] [PubMed]

8. Protesescu, L.; Yakunin, S.; Bodnarchuk, M.I.; Krieg, F.; Caputo, R.; Hendon, C.H.; Yang, R.X.; Walsh, A.; Kovalenko, M.V. Nanocrystals of cesium lead halide perovskites ($CsPbX_3$, X = Cl, Br, and I): Novel optoelectronic materials showing bright emission with wide color gamut. *Nano Lett.* **2015**, *15*, 3692–3696. [CrossRef] [PubMed]

9. Nedelcu, G.; Protesescu, L.; Yakunin, S.; Bodnarchuk, M.I.; Grotevent, M.J.; Kovalenko, M.V. Fast anion-exchange in highly luminescent nanocrystals of cesium lead halide perovskites ($CsPbX_3$, X = Cl, Br, I). *Nano Lett.* **2015**, *15*, 5635–5640. [CrossRef] [PubMed]

10. Zhang, D.; Yang, Y.; Bekenstein, Y.; Yu, Y.; Gibson, N.A.; Wong, A.B.; Eaton, S.W.; Kornienko, N.; Kong, Q.; Lai, M.; et al. Synthesis of composition tunable and highly luminescent cesium lead halide nanowires through anion-exchange reactions. *J. Am. Chem. Soc.* **2016**, *138*, 7236–7239. [CrossRef] [PubMed]

11. Vybornyi, O.; Yakunin, S.; Kovalenko, M.V. Polar-solvent-free colloidal synthesis of highly luminescent alkylammonium lead halide perovskite nanocrystals. *Nanoscale* **2016**, *8*, 6278–6283. [CrossRef] [PubMed]

12. Huang, H.; Polavarapu, L.; Sichert, J.A.; Susha, A.S.; Urban, A.S.; Rogach, A.L. Colloidal lead halide perovskite nanocrystals: Synthesis, optical properties and applications. *NPG Asia Mater.* **2016**, *8*, e328. [CrossRef]

13. Luo, B.; Pu, Y.-C.; Yang, Y.; Lindley, S.A.; Abdelmageed, G.; Ashry, H.; Li, Y.; Li, X.; Zhang, J.Z. Synthesis, optical properties, and exciton dynamics of organolead bromide perovskite nanocrystals. *J. Phys. Chem. C* **2015**, *119*, 26672–26682. [CrossRef]

14. Tyagi, P.; Arveson, S.M.; Tisdale, W.A. Colloidal organohalide perovskite nanoplatelets exhibiting quantum confinement. *J. Phys. Chem. Lett.* **2015**, *6*, 1911–1916. [CrossRef] [PubMed]

15. Akkerman, Q.A.; Park, S.; Radicchi, E.; Nunzi, F.; Mosconi, E.; De Angelis, F.; Brescia, R.; Rastogi, P.; Prato, M.; Manna, L. Nearly monodisperse insulator Cs_4PbX_6 (X = Cl, Br, I) nanocrystals, their mixed halide compositions, and their transformation into $CsPbX_3$ nanocrystals. *Nano Lett.* **2017**, *17*, 1924–1930. [CrossRef] [PubMed]

16. Noh, J.H.; Im, S.H.; Heo, J.H.; Mandal, T.N.; Seok, S.I. Chemical management for colorful, efficient, and stable inorganic-organic hybrid nanostructured solar cells. *Nano Lett.* **2013**, *13*, 1764–1769. [CrossRef] [PubMed]

17. Johnston, M.B.; Herz, L.M. Hybrid perovskites for photovoltaics: charge-carrier recombination, diffusion, and radiative efficiencies. *Acc. Chem. Res.* **2016**, *49*, 146–154. [CrossRef] [PubMed]

18. Liu, Y.; Yang, Z.; Cui, D.; Ren, X.; Sun, J.; Liu, X.; Zhang, J.; Wei, Q.; Fan, H.; Yu, F.; et al. Two-inch-sized perovskite $CH_3NH_3PbX_3$ (X = Cl, Br, I) crystals: Growth and characterization. *Adv. Mater.* **2015**, *27*, 5176–5183. [CrossRef] [PubMed]

19. Fitzmorris, B.C.; Pu, Y.C.; Cooper, J.K.; Lin, Y.F.; Hsu, Y.J.; Li, Y.; Zhang, J.Z. Optical properties and exciton dynamics of alloyed core/shell/shell $Cd_{(1-X)}Zn_{(X)}Se/ZnSe/ZnS$ quantum dots. *ACS Appl. Mater. Interfaces* **2013**, *5*, 2893–2900. [CrossRef] [PubMed]

20. Zeng, R.; Zhang, T.; Dai, G.; Zou, B. Highly emissive, color-tunable, phosphine-free Mn:ZnSe/ZnS core/shell and Mn:ZnSeS shell-alloyed doped nanocrystals. *J. Phys. Chem. C* **2011**, *115*, 3005–3010. [CrossRef]

21. Begum, R.; Parida, M.R.; Abdelhady, A.L.; Murali, B.; Alyami, N.M.; Ahmed, G.H.; Hedhili, M.N.; Bakr, O.M.; Mohammed, O.F. Engineering interfacial charge transfer in $CsPbBr_3$ perovskite nanocrystals by heterovalent doping. *J. Am. Chem. Soc.* **2017**, *139*, 731–737. [CrossRef] [PubMed]

22. Liu, M.; Zhong, G.; Yin, Y.; Miao, J.; Li, K.; Wang, C.; Xu, X.; Shen, C.; Meng, H. Aluminum-doped cesium lead bromide perovskite nanocrystals with stable blue photoluminescence used for display backlight. *Adv. Sci.* **2017**, 1700335. [CrossRef] [PubMed]

23. Van der Stam, W.; Geuchies, J.J.; Altantzis, T.; van den Bos, K.H.; Meeldijk, J.D.; Van Aert, S.; Bals, S.; Vanmaekelbergh, D.; de Mello Donega, C. Highly emissive divalent-ion-doped colloidal $CsPb_{1-x}M_xBr_3$ perovskite nanocrystals through cation exchange. *J. Am. Chem. Soc.* **2017**, *139*, 4087–4097. [CrossRef] [PubMed]

24. Lin, C.C.; Xu, K.Y.; Wang, D.; Meijerink, A. Luminescent manganese-doped $CsPbCl_3$ perovskite quantum dots. *Sci. Rep.* **2017**, *7*, 45906. [CrossRef] [PubMed]

25. Parobek, D.; Roman, B.J.; Dong, Y.; Jin, H.; Lee, E.; Sheldon, M.; Son, D.H. Exciton-to-dopant energy transfer in mn-doped cesium lead halide perovskite nanocrystals. *Nano Lett.* **2016**, *16*, 7376–7380. [CrossRef] [PubMed]

26. Das Adhikari, S.; Dutta, S.K.; Dutta, A.; Guria, A.K.; Pradhan, N. Chemically tailoring the dopant emission in Manganese-doped $CsPbCl_3$ perovskite nanocrystals. *Angew. Chem.* **2017**, *56*, 8746–8750. [CrossRef] [PubMed]

27. Huang, G.; Wang, C.; Xu, S.; Zong, S.; Lu, J.; Wang, Z.; Lu, C.; Cui, Y. Postsynthetic doping of $MnCl_2$ molecules into preformed $CsPbBr_3$ perovskite nanocrystals via a halide exchange-driven cation exchange. *Adv. Mater.* **2017**, *29*. [CrossRef] [PubMed]

28. Liu, H.; Wu, Z.; Shao, J.; Yao, D.; Gao, H.; Liu, Y.; Yu, W.; Zhang, H.; Yang, B. $CsPb_xMn_{1-x}Cl_3$ perovskite quantum dots with high mn substitution ratio. *ACS Nano* **2017**, *11*, 2239–2247. [CrossRef] [PubMed]

29. Wang, Q.; Zhang, X.; Jin, Z.; Zhang, J.; Gao, Z.; Li, Y.; Liu, S.F. Energy-Down-Shift $CsPbCl_3$: Mn quantum dots for boosting the efficiency and stability of perovskite solar cells. *ACS Energy Lett.* **2017**, *2*, 1479–1486. [CrossRef]

30. Mir, W.J.; Jagadeeswararao, M.; Das, S.; Nag, A. Colloidal mn-doped cesium lead halide perovskite nanoplatelets. *ACS Energy Lett.* **2017**, 537–543. [CrossRef]

31. Liu, W.; Lin, Q.; Li, H.; Wu, K.; Robel, I.; Pietryga, J.M.; Klimov, V.I. Mn^{2+}-doped lead halide perovskite nanocrystals with dual-color emission controlled by halide content. *J. Am. Chem. Soc.* **2016**, *138*, 14954–14961. [CrossRef] [PubMed]

32. Shamsi, J.; Dang, Z.; Bianchini, P.; Canale, C.; Stasio, F.D.; Brescia, R.; Prato, M.; Manna, L. colloidal synthesis of quantum confined single crystal $CsPbBr_3$ nanosheets with lateral size control up to the micrometer range. *J. Am. Chem. Soc.* **2016**, *138*, 7240–7243. [CrossRef] [PubMed]

33. Bekenstein, Y.; Koscher, B.A.; Eaton, S.W.; Yang, P.; Alivisatos, A.P. Highly luminescent colloidal nanoplates of perovskite cesium lead halide and their oriented assemblies. *J. Am. Chem. Soc.* **2015**, *137*, 16008–16011. [CrossRef] [PubMed]

34. Luo, B.; Pu, Y.C.; Lindley, S.A.; Yang, Y.; Lu, L.; Li, Y.; Li, X.; Zhang, J.Z. Organolead halide perovskite nanocrystals: Branched capping ligands control crystal size and stability. *Angew. Chem.* **2016**, *55*, 8864–8868. [CrossRef] [PubMed]

35. Sun, C.; Zhang, Y.; Ruan, C.; Yin, C.; Wang, X.; Wang, Y.; Yu, W.W. Efficient and stable white leds with silica-coated inorganic perovskite quantum dots. *Adv. Mater.* **2016**, *28*, 10088–10094. [CrossRef] [PubMed]

36. Moller, C.K. A phase transition in cesium plumbochloride. *Nature* **1957**, *180*, 981–982. [CrossRef]

37. Rossi, D.; Parobek, D.; Dong, Y.; Son, D.H. Dynamics of exciton-mn energy transfer in mn-doped $CsPbCl_3$ perovskite nanocrystals. *J. Phys. Chem. C* **2017**, *121*, 17143–17149. [CrossRef]

38. Guria, A.K.; Dutta, S.K.; Adhikari, S.D.; Pradhan, N. Doping Mn^{2+} in lead halide perovskite nanocrystals: Successes and challenges. *ACS Energy Lett.* **2017**, *2*, 1014–1021. [CrossRef]

39. Zou, S.; Liu, Y.; Li, J.; Liu, C.; Feng, R.; Jiang, F.; Li, Y.; Song, J.; Zeng, H.; Hong, M.; et al. Stabilizing cesium lead halide perovskite lattice through Mn(II) substitution for air-stable light-emitting diodes. *J. Am. Chem. Soc.* **2017**, *139*, 11443–11450. [CrossRef] [PubMed]